JOURNAL OF THERMOPHYSICS AND HEAT TRANSFER
Vol. 24, No. 1, January–March 2010

Novel Semi-Empirical Model for Finite Rate Catalysis with Application to PM1000 Material

S. Di Benedetto*
Italian Aerospace Research Center, 81043 Capua, Italy
and
C. Bruno†
University of Rome "La Sapienza," 00184 Rome, Italy

DOI: 10.2514/1.44552

A simplified model for heterogeneous catalysis is presented. A theoretical expression of the recombination coefficient has been obtained by means of an analogy with gas-phase kinetics, whereby desorption is assumed similar to final product formation following decomposition of the activated compound. The constants of the model are defined by fitting experimental data. The method devised is particularly useful when detailed physical modeling approaches are unrealizable, namely when material characteristics are unknown. This model has been applied to PM1000, the material planned for the ESA EXPERT capsule external skin. The expression of the recombination coefficient has been interpolated using the experimental data provided by the Centre National de la Recherche Scientifique in France and the von Karman Institute in Belgium, implemented in the Centro Italiano Ricerche Aerospaziali computational fluid dynamics code, and tested for typical reentry conditions. Its application to the EXPERT capsule reentry problem shows that it appears to work well and is promising. Results confirm the importance of realistically modeling catalytic recombination on thermal protection systems, both in terms of wall heat flux and chemical composition of the airstream near the surface. In particular, the heat flux predicted is much lower than in the case of fully catalytic surface, indicating that, at the points of the EXPERT trajectory chosen, PM1000 seems to have poor catalytic activity.

Nomenclature

A, B	=	chemical species
$[A]$, $[B]$	=	concentration of chemical species
a_n	=	constants
D_d	=	downstream influence
D_u	=	upstream influence
E_n	=	activation energy of the process n
$f_{h=0}$	=	Richardson extrapolation
f_i	=	value computed on the grid point i
h	=	altitude
K_i	=	rate of production of the species i
k	=	Boltzmann constant
k_{nf}	=	forward reaction rate coefficient of step n
k_{nr}	=	reverse reaction rate coefficient of step n
Li	=	grid levels
M	=	Mach number
N	=	number of cells
P	=	pressure
p	=	order of convergence
Re	=	Reynolds number
R_u	=	universal gas constant
r	=	grid refinement ratio
T	=	temperature
v	=	entry velocity
W_i	=	molecular weight of species i
Y_i	=	mass fraction of species i
β	=	chemical energy accommodation coefficient
γ	=	effective recombination coefficient
γ_i	=	recombination coefficient of species i
Δy_w	=	minimum spacing normal to the wall at the stagnation point
ε	=	surface emissivity coefficient

Subscripts

diff	=	diffusive
f	=	forward
i	=	chemical species
r	=	reverse
w	=	wall

Superscript

$*$	=	activated or adsorbed

Received 24 March 2009; revision received 30 July 2009; accepted for publication 11 August 2009.

*Research Engineer, Department of Aerothermodynamics and Space Propulsion, Via Maiorise.

†Professor, Dipartimento di Meccanica e Aeronautica, Via Eudossiana 18. Associate Fellow AIAA.

I. Introduction

CATALYTIC recombination during hypersonic flight is driven by the presence of oxygen, nitrogen atoms, and NO formed from the bow shock. These species cross the boundary layer, reach the surface of the vehicle, at temperatures between 300 and 2000 K, and recombine there, depositing heat and contributing to the total surface heat flux.

Convincing estimates of the heat flux contribution due to catalysis indicate it may constitute up to 40% of the total heat flux on the thermal protection system (TPS) surface near the stagnation point [1]. Hence, the need to understand catalytic finite-rate recombination.

Material-dependent numerical models and calculations of catalytic recombination have been developed, using different approaches [2–8]. A common issue with all models is the need for validation, which can be accomplished only by means of reliable experimental measurements; these are also fundamental to improve knowledge of catalysis physics and thus for its modeling.

Ideally, the data needed to test a recombination model are concentrations of O, N, and NO or, with appropriate assumptions, heat fluxes as well as temperature and pressure, all taken at the same

point of the TPS surface. Unfortunately, measuring anything in hypersonic boundary layers over a reentering craft is very hard, and no such consistent set of data exists. Faced with this problem, it is expedient to test and validate models using whatever data may be available in the open literature, including ground facilities and flight data, if any.

When the TPS material is not known or poorly characterized, such detailed modeling cannot be performed; however, if reasonably accurate measurements are available, one can use them "as they are," assuming typically broad margins. An alternative approach is described next.

II. Simplified Catalytic Recombination Model

If experimental recombination coefficients exist, what one generally does is to fit them by linear interpolation or in Arrhenius form. This latter, however, best describes a *single step* homogeneous reaction and therefore is conceptually not suitable to describe a catalytic process. The alternative involving somewhat plausible physics is described in the following.

The starting point is the assumption that interaction between a gas-phase atom and a surface may be described by kinetics mimicking that between gas-phase species. This approach is consistent with Langmuir–Hinshelwood (L.-H.) recombination, and, to a lesser degree, with Eley–Rideal (E.-R.) recombination kinetics.

In this context, L.-H. recombination is treated as gas-phase chemistry, except the reactants move much more slowly (the reaction cross section should therefore be larger). Desorption becomes then akin to product(s) formation following the decomposition of the activated complex. The term activated complex refers to the molecular compound or compounds that exist in the highest energy state, or activated stage, during a chemical reaction [9]. An activated complex $(\,)^*$ acts as an intermediary between the reactants and the products of the reaction, as in the following example:

$$A + B \rightarrow (C)^* \qquad (C)^* \rightarrow C + D \tag{1}$$

Therefore, a generic chemical reaction goes through three stages, the initial stage consisting of the reactants, the transition stage of the activated complex, and the final stage, in which the products are formed. In essence, for instance, an E.-R. recombination process can be summarized as follows:

$$A + A^* \underset{K_{1r}}{\overset{K_{1f}}{\rightleftarrows}} (AA^*)^* \overset{K_2}{\rightarrow} A_2 \tag{2}$$

where k_n are the reaction rate coefficients and the subscripts f and r indicate forward and reverse reaction direction. The symbol $(\,)^*$ means activated in homogeneous chemistry, whereas in catalysis, it is understood to mean adsorbed.

The formation rate of $(AA^*)^*$ in Eq. (2) is

$$\frac{\mathrm{d}[(AA^*)^*]}{\mathrm{d}t} = k_{1f}[A][A^*] - k_{1r}[(AA^*)^*] - k_2[(AA^*)^*] = k_{1f}[A][A^*] - (k_{1r} + k_2)[(AA^*)^*] \tag{3}$$

The crucial assumptions at this point are 1) that each of the elementary steps influences the rate; therefore, all of the steps must be accounted for in calculating the rate equation, and 2) that the concentration of the intermediate $(AA^*)^*$ does not change with time, that is, there is no accumulation of the activated compound (Lindemann's hypothesis):

$$\frac{\mathrm{d}[(AA^*)^*]}{\mathrm{d}t} = 0 \tag{4}$$

Substituting this condition in Eq. (3), the concentration of the compound $(AA^*)^*$ can be immediately found:

$$[(AA^*)] = \frac{k_{1f}}{k_{1r} + k_2}[A][A^*] \tag{5}$$

On the other hand, from Eq. (2), we have

$$\frac{\mathrm{d}[A_2]}{\mathrm{d}t} = k_2[(AA^*)] \tag{6}$$

and, finally, substituting Eq. (5) in Eq. (6),

$$\frac{\mathrm{d}[A_2]}{\mathrm{d}t} = \frac{k_2 k_{1f}}{k_{1r} + k_2}[A][A^*] \tag{7}$$

Each reaction coefficient k_i is supposed to follow an Arrhenius dependence form, so that, in Eq. (7),

$$\frac{k_2 k_{1f}}{k_{1r} + k_2} = \frac{a_2 a_{1f} \exp(\frac{-E_{1f}-E_2}{R_u T})}{a_{1r} \exp(\frac{-E_{1r}}{R_u T}) + a_2 \exp(\frac{-E_2}{R_u T})} \tag{8}$$

where E_n indicates the activation energy of each step and R_u the universal gas constant (=8.3145 J mole^{-1} K^{-1}).

This reaction rate is related to the recombination coefficient γ_i by means of the Hertz–Knudsen relation:

$$K_i = \gamma_i \sqrt{\frac{kT}{2\pi W_i}} \tag{9}$$

where here k is the Boltzmann constant ($1.38066\,10^{-23}$ J/K) and W_i the molecular weight of the species i.

Finally, combining Eqs. (8) and (9), the analytical expression for the recombination coefficient is

$$\gamma_i = \frac{1}{\sqrt{\frac{kT}{2\pi W_i}}} \frac{a_2 a_{1f} \exp(\frac{-E_{1f}-E_2}{R_u T})}{a_{1r} \exp(\frac{-E_{1r}}{R_u T}) + a_2 \exp(\frac{-E_2}{R_u T})} \tag{10}$$

Note that this expression *does* contain Arrhenius-type exponentials, but *does not behave* as an Arrhenius term. The same approximation yields the catalytic recombination of the L.-H. type.

The relation (10) expresses $\gamma_i(T)$ as function of six constants to be determined, and can be used to fit sets of experimental data.

III. Application to the PM1000 Material

The preceding model has been tested on the PLANSEE PM1000® material, a metallic alloy consisting mainly of nickel with a high content of chrome (about 20%) and small quantities of other metals.

Work has been sponsored by ESA to find the catalyticity of PM1000, the material planned for the thermal protection system of the EXPERT capsule hull. This material is much more structurally complex than silica or other ceramics, partly due to the alloy and partly due to the microcrystalline structure (crystallites of PM1000 in pictures from [10–13] show major changes with temperature and test duration). Moreover, information concerning this material is proprietary, so that even the simplest data, for example, its raw composition, are unknown.

We have only experimental measurements of the recombination coefficient of this material; they have been obtained separately and with different techniques at (VKI) (see [10,13,14]) and at the Centre National de la Recherche Scientifique (CNRS) (see [15,16]). Both data refer to preoxidized material, but whereas CNRS tested a pure oxygen stream and then measured only oxygen recombination γ_O, VKI tested PM1000 in an airstream and measured the effective catalyticity γ assuming it is the same for all species.

The relatively low melting point (about 1600 K) of this Cr-rich alloy limits its use only in low-Earth-orbit reentry, where the contribution of N recombination to the overall wall heat transfer flux HT_w is much less than that of O.

A. Experimental Data

The experimental data available report γ (VKI) and γ_O (CNRS) as a function of T at different pressures, see Table 1. The data are plotted in Fig. 1 (VKI) and Fig. 2 (CNRS).

In the work done at the VKI, the heat flux contribution due to recombination has been extracted from the raw HT_w measurements

Table 1 Pressure considered in the experiments

	Pressure, Pa
CNRS	300; 1000
VKI	1500; 5000; 10,000; 20,000

by subtracting those due to radiation and convection: these two were obtained not from simultaneous measurements (unfeasible), but by calculations after simulating the subsonic flow with a boundary-layer code. Thus, this γ is the byproduct of combining together data and modeling.

The 2004 campaign at VKI tested PM1000 up to close to the melting point; in fact, some sample had melting problems, and it is advisable not to consider reliable the corresponding γ. All other tests were limited to 1500 K.

A new campaign (2007, [13]) repeated the 2004 tests with an improved methodology. The two sets of γ show up to 1 order of magnitude difference. An evaluation of the possible cause of uncertainties (heat flux measurements, emissivity, etc.) is provided in the earlier reports; the final report of the last campaign also includes error estimates. The two datasets (2004 and 2007) at the same pressure (10.000 Pa) are reported in Fig. 3, showing the older data within the new error bars.

In 2005, parallel work was carried out by Balat-Pichelin and Badie at the Moyen d'Essai Solaire d'Oxydation (MESOX) facility of CNRS [16]. These measurements are not based on heat fluxes, but are optical, that is, direct O-emission measurement in the boundary layer above the material. The overall accuracy on the recombination coefficient is given as $\pm 30\%$. Two pressures were tested: 300 and 1000 Pa. The data at 300 Pa are in turn divided into two subgroups; the ones tagged pm9 refer to samples used first to study the effect of air plasma by looking for emission of species due to oxidation in the gas phase above the sample. A larger recombination coefficient was observed, this fact probably being an indication of a more oxidized material, as observed in [16].

The variation of catalytic behavior of a material with oxidation depends on the kind of oxide which forms and then is different from material to material. The situation is more complex when the material is an alloy, as in the case of PM1000, because the oxide layer is composed of different kinds of oxides. For PM1000, the oxide layer is mainly composed of Cr_2O_3.

In [16], Balat-Pichelin and Badie report that looking at the micrographs of the three PM1000 samples tested in the MESOX facility, the primary oxidation layer due to manufacturing of the samples shows small crystallites in pm11 and pm10 and large crystallites in pm9. The latter are similar to those present on Cr_2O_3 samples; from this, the suspicion that the pm9 sample was probably more oxidized.

The range of temperature covered by CNRS is broader than that at VKI, and temperatures lie well above the 1500 K imposed by VKI to avoid sample melting; in fact the maximum temperature tested by CNRS is 1647 K and no melting of the sample was observed. This might be due to the short time of exposure, but there is also a difference in the temperature diagnostics, by means of a dual-color pyrometry at VKI and by single-color at CNRS. In the latter case, the emissivity is assumed and constant with temperature, so it is

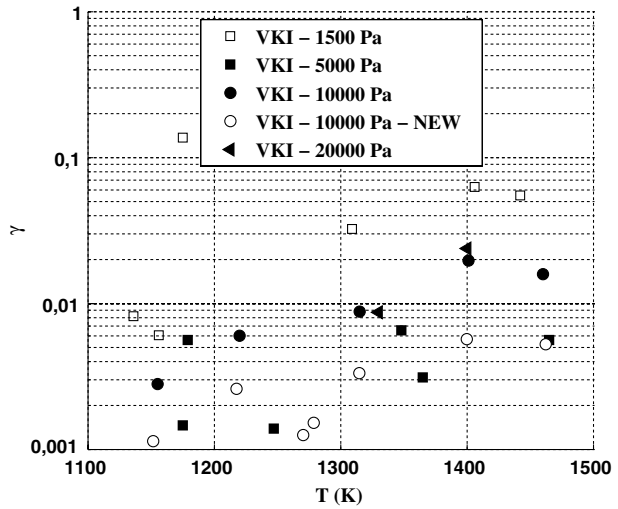

Fig. 1 VKI experimental measurements.

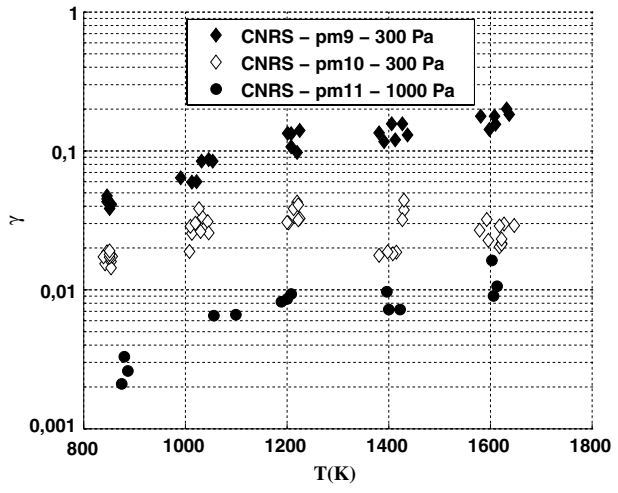

Fig. 2 CNRS experimental measurements.

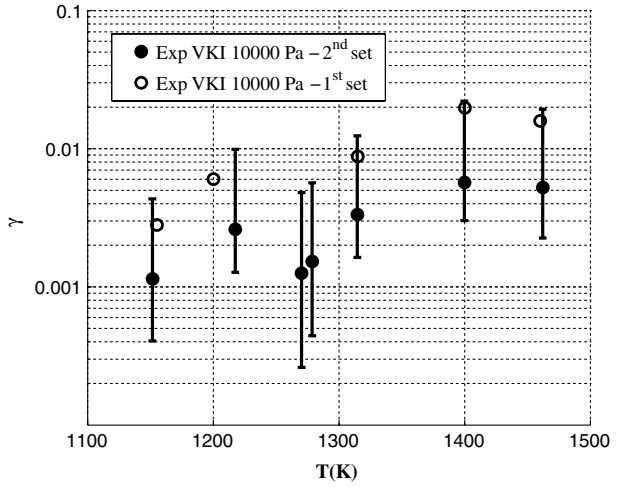

Fig. 3 Comparison between data at 10,000 Pa.

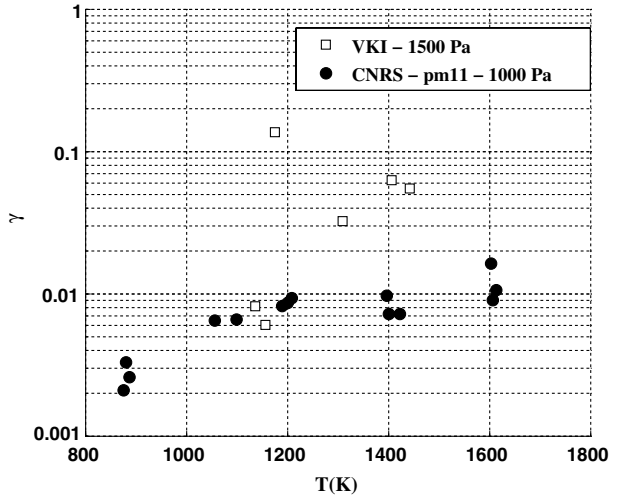

Fig. 4 Comparison between VKI and CNRS results at similar pressures.

expected that temperatures measured by CNRS are affected by a greater uncertainty with respect to those reported by VKI.

Comparison between the two γ obtained by VKI and by CNRS is shown in Fig. 4 at pressure 1500 and 1000 Pa, respectively. This comparison shows CNRS γ are 1 order of magnitude lower than those reported by VKI.

However, Balat-Pichelin and Badie [16] suggested caution in drawing conclusions from the CNRS datasets, due to a probably wrong assumption on the gas temperature. To further add to an already complicated situation, all the data mentioned so far are lower than those by Stewart and Bouslog at 36 Pa [17], including a 2 orders of magnitude difference in the range 800–1250 K.

Concerning the recombination coefficient trend with pressure, up to 5000 Pa there is an inverse proportionality between the two; this trend inverts at higher pressure. Recall that recombination depends on diffusivity and on collision frequency, both related to pressure in opposite ways. Looking at all these data, one is led to think that, at low pressure, diffusivity is controlling, while at higher pressure, the dominant effect is that related to collisions.

From all the observations made, the following must be kept in mind:

1) The recombination coefficient has a different meaning in the CNRS and in the VKI data: the former is linked to direct oxygen concentration measurement, and the latter to a heat flux (indirect measurement). This means that what is measured by CNRS is the recombination probability γ_i, whereas VKI measures the so-called effective recombination coefficient γ, defined as $\gamma_i\beta$, where β is the chemical energy accommodation coefficient. Therefore, the data should not be directly compared;

2) Even though the VKI data explore a wider range of pressures, only a few values of γ are provided for each of them. Thus interpolation is more complicated and likely less reliable, as it will be shown in the following.

Finally, from both campaigns, it emerges that accurate knowledge of the oxidation state is very important, as it boosts oxygen recombination, leading to higher recombination coefficients, as intuitively expected.

For what has been said, and in accord with the authors themselves, it is clear that the experimental data collected until now cannot be used for a realistic characterization of the catalyticity of PM1000. Academically speaking, however, they provide a good application of the correlation in Eq. (10).

B. Fitting the Experimental Data

Data fitting has been performed by means of the Curve Fitting Toolbox of MATLAB® [18]. It uses the nonlinear least-squares formulation to fit a nonlinear model to data by means of a custom equation.

In nonlinear models, the coefficients cannot be estimated using simple matrix techniques, instead an iterative approach is required that follows these steps:

1) Estimate initially each interpolating coefficient.

2) Generate a fitted curve for the current set of coefficients.

3) Adjust coefficients to determine whether the fit improves, by means of a fitting algorithm.

4) Iterate by returning to step 2, until the fit reaches a specified convergence.

The algorithm chosen for item 3 is the "trust-region"[19] by which it is possible to specify coefficient constraints; for example, in this particular case, a lower positive bound for the activation energies has been imposed. Moreover, this algorithm can solve difficult nonlinear problems more efficiently than others, being an improvement of the Levenberg–Marquardt algorithm [19]. To minimize the influence of outliers, a robust least-squares regression has been used: least absolute residuals method, or "bisquare weights," depending on the case. Finally, the best fit parameters have been evaluated by examining both the visual (looking at the residuals, which for a good fit should look random, with no apparent pattern) and numerical (sum of squares due to error, sum of square of the regression, fit standard error) results of the fit.

All this has been carried out for each pressure of Table 1; because six constants must be defined in the γ expression, at least six data are necessary. Thus, the VKI data at 20,000 Pa have not been processed and the old set at 10,000 Pa (excluding the sample where incipient melting was observed) has been joined with the new set at the same pressure.

It is clear that, although a numerical solution is possible with just six data, the "goodness" of the fit was unlikely to be high, mainly because of data scatter (e.g., see data at 1500 and 5000 Pa). The Curve Fitting Toolbox provides prediction bounds for the fitted function. The bounds are associated with a level of certainty to be specified (for example, 95% has been used in this case) and that define an interval around the fitted function. This interval indicates that there is a 95% chance that a new observation is actually within the lower and upper prediction bounds. Therefore, a wide interval for the fitted coefficients is a clear indication that more data are necessary.

Results in terms of the interpolating function are shown from Figs. 5–9; Fig. 5 also shows the prediction bounds. For the fit at 10,000 Pa (Fig. 9), greater weight has been assigned to the 2007 data [13], as they *should* be more reliable. The corresponding set of coefficients for Eq. (10) are listed, at each pressure, in Table 2.

IV. Porting the PM1000 Model on a Computational Fluid Dynamics Code

To introduce the PM1000 model in the computational fluid dynamics simulating the hypersonic flowfield, pressure dependence must be introduced in Eq. (10).

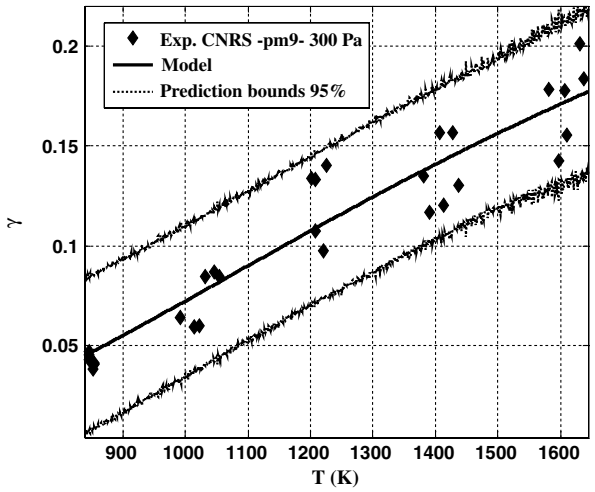

Fig. 5 CNRS dataset at 300 Pa (pm9 sample) [16], fit obtained with this model and prediction bounds.

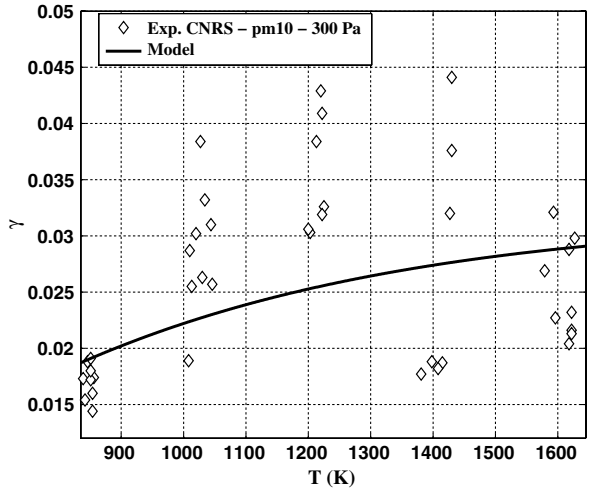

Fig. 6 CNRS dataset at 300 Pa (pm10 sample) [16] and fit obtained with this model.

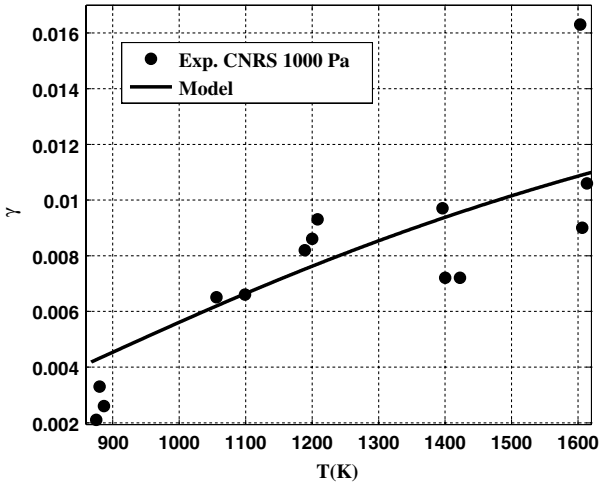

Fig. 7 CNRS dataset at 1000 Pa [16] and fit obtained with this model.

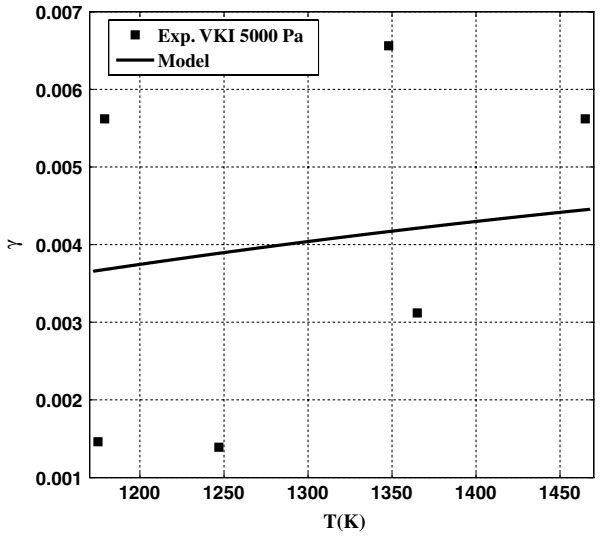

Fig. 8 VKI dataset at 5000 Pa [11] and fit obtained with this model.

There are different possible ways to do this. One is to define a function for γ where each coefficient is a function of pressure by interpolating the data in Table 2 (an example is shown in Fig. 10 for the coefficient a_{1f}) and then substituting these functions in Eq. (10).

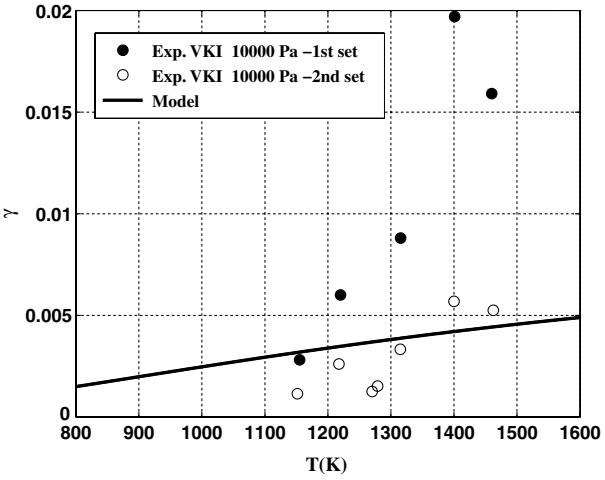

Fig. 9 VKI dataset at 10,000 Pa (2004 and 2007 [11,13]) and fit obtained with this model.

However, this procedure has some drawbacks. In fact, because the relation describing the coefficients (and obviously also the total γ) is an unknown function of pressure, and because the dependence of γ on the coefficients is nonlinear, there are too many degrees of freedom in building the function $\gamma_i = \gamma_i(T, P)$, and the risk does exist to predict completely wrong values. A way to reduce the risk is to use a nonoscillating interpolating function assuming the values of the coefficients defined for each pressure in Table 2. An example is a piecewise linear *function*, consistent with the γ modeled in the previous section. A simpler alternative is to use a piecewise linear *interpolation* of the functions $\gamma_i = \gamma_i(T, \bar{P})$, where $\bar{P}$ is the pressure for which the experimental data exist. In this way, at least the γ behavior at each experimental pressure is reproduced correctly.

Both solutions have been tried (see Sec. V), and the first one adopted for the last test case. In fact, this choice should be evaluated case by case, according to the type of experimental data available.

The Centro Italiano Ricerche Aerospaziali (CIRA) code H3NS has been used to perform two-dimensional, axisymmetric computations.

H3NS is a structured multiblock finite volume solver that allows for the treatment of a wide range of compressible fluid dynamic problems and has been widely validated in the past [20,21]. It solves the full Navier–Stokes equations for a real gas in thermal and chemical nonequilibrium conditions. The governing equations, written in conservation form, are discretized by using a finite volume technique with a centered formulation; the inviscid fluxes are computed by means of a flux difference splitting Riemann solver, with a second order essentially nonoscillatory reconstruction of interface values, whereas viscous fluxes are calculated by central differencing, that is, computing the gradients of flow variables at cell interfaces by means of the Gauss theorem. Time integration is performed with an explicit Euler forward algorithm and a local time stepping formulation, coupled with a point-implicit evaluation of chemistry and vibrational source terms.

In the case of thermochemical nonequilibrium flows, the fluid is treated as a mixture of perfect gases. The chemical model for air is due to Park [25] and it is characterized by 17 reactions between the five species (O, N, NO, O_2, N_2), neglecting the presence of inert gas or water in the air. The energy exchange between vibrational and translational modes is modeled with the classical Landau–Teller nonequilibrium equation, with relaxation times taken from the Millikan–White theory [26] modified by Park [27]. The viscosity of the single species is evaluated by a fit of collision integrals calculated by Yun and Mason [28]; the thermal conductivity is calculated by means of the Eucken law; the viscosity and thermal conductivity of the gas mixture are then calculated with the semi-empirical Wilke's formulas. The diffusion of the multicomponent gas is computed through a sum rule of the binary diffusivities of each couple of species [29]. Transport coefficients, assuming ideal gas, are derived from Sutherland's law.

V. Test Cases

The behavior of the semi-empirical catalysis model has been verified by means of two test cases: a sphere-cylinder exposed to a plasma flow, and the EXPERT capsule in flight conditions, for which PM1000 is to be the TPS material of choice.

The PM1000 model has been tested in two versions (see Sec. IV): in the first, the pressure dependence is obtained by interpolating the functions $\gamma_i = \gamma_i(T, \bar{P})$ and, in the following, this version will be indicated with $a_n(T)$. In the second version, each coefficient of γ has been interpolated as a function of pressure. This version will be indicated with $a_n(P, T)$. The two approaches give very similar results (as shown later).

Because of the lack of experimental measurements of the catalytic formation of N_2 and NO molecules, this model only accounts for the γ_O recombination coefficient. The recombination probability γ_N has been considered equal to γ_O to be consistent with VKI in extracting their measurements, but also the two limit conditions of fully catalytic and noncatalytic walls have been used to evaluate for the

Table 2 Final coefficients defining the interpolating functions

	P, Pa	a_{1f}, s^{-1}	a_{1r}, s^{-1}	a_2, s^{-1}	E_{1f}, J/mol	E_{1r}, J/mol	E_2, J/mol
CNRS	300	4.096E − 04	2.833E + 05	6.758E − 04	24920.000	48570.000	34650.000
CNRS	300 (pm9)	5.264E − 08	3.869E + 07	1.152E + 04	13520.000	10010.000	20740.000
CNRS	1000	2.85E − 04	1.22E + 05	3.06E − 04	15020.000	10170.000	15020.000
VKI	5000	1.92E − 04	5.01E + 04	5.00E − 05	15000.000	15000.000	15000.000
VKI	10,000	1.00E − 04	1.52E + 04	5.10E − 05	15240.000	10080.000	15240.000

formation of N_2. The surface has been considered noncatalytic with respect to NO.

Radiative equilibrium has been imposed in both cases as the boundary condition for the energy equation with emissivity coefficient $\varepsilon = 0.8$. The flow is supposed in thermochemical nonequilibrium.

A. Sphere-Cylinder in Plasma Wind-Tunnel Test Case

A sphere-cylinder of 10 cm diameter has been exposed to an axial-symmetric plasma flow; asymptotic conditions are typical of the Scirocco Plasma Wind Tunnel at CIRA and are reported as $M=$ 7.938, $T = 648.56$ K, $P = 41.75$ Pa, $Y_O = 0.2329$, $Y_N = 0.038$, $Y_{NO} = 1.62$E-5, and $Y_{O_2} = 6.07$E-5. Y_i are the species mass fractions.

Three grid levels have been adopted to prove grid independence of results [22]. Results shown hereinafter are related to the medium grid level, which is shown in Fig. 11.

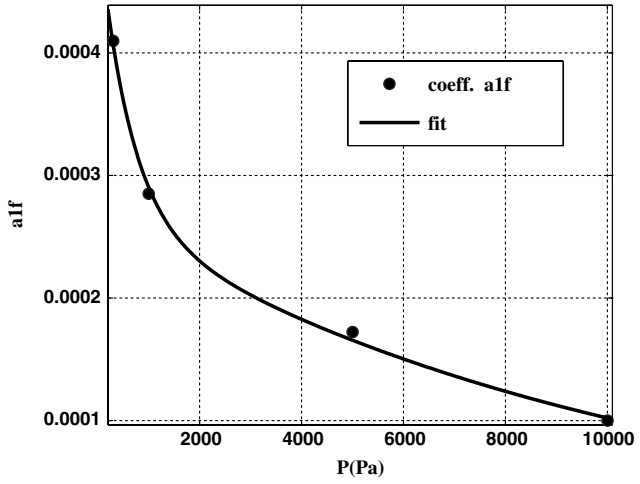

Fig. 10 Coefficient a_{1f} as function of pressure.

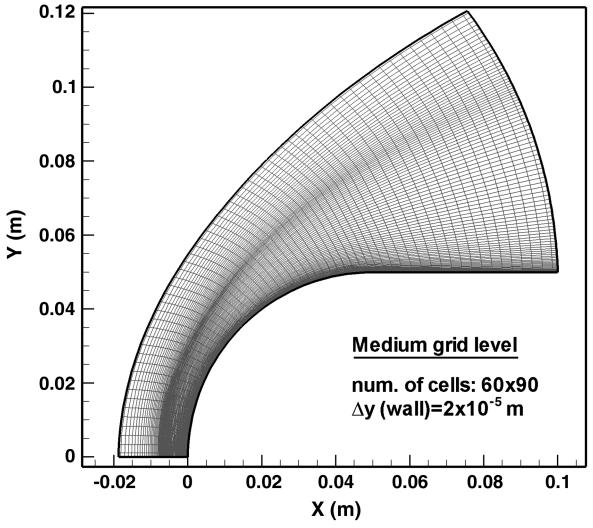

Fig. 11 Computational grid.

In Fig. 12, mass fraction profiles of the five species are plotted along the stagnation line, in the cases of equal recombination probability for O and N (dash-dot line), complete wall nitrogen recombination (dashed line), and no catalytic nitrogen recombination (solid line).

The stagnation region is enlarged in Fig. 13. It is worth noticing that what occurs on the surface is strongly coupled to the gas field. In fact, the species that form at the wall diffuse in the flow promoting air chemistry reactions. For example, the gas-phase reaction $N_2 + O \rightarrow NO + N$ is promoted by the presence of nitrogen molecules diffusing from the surface when $\gamma_N \neq 0$.

The two versions of the semi-empirical model, with the two versions of pressure dependence, and in the three cases $\gamma_N = \gamma_O$, $\gamma_N = 1$, and $\gamma_N = 0$ are compared in Figs. 14 and 15. The two versions produce more or less the same results, whereas the recombination of nitrogen atoms plays a very important role, implying an increase of total wall heat flux at the stagnation point of about 53% for $\gamma_N = 1$ with respect to the noncatalytic case $\gamma_N = 0$.

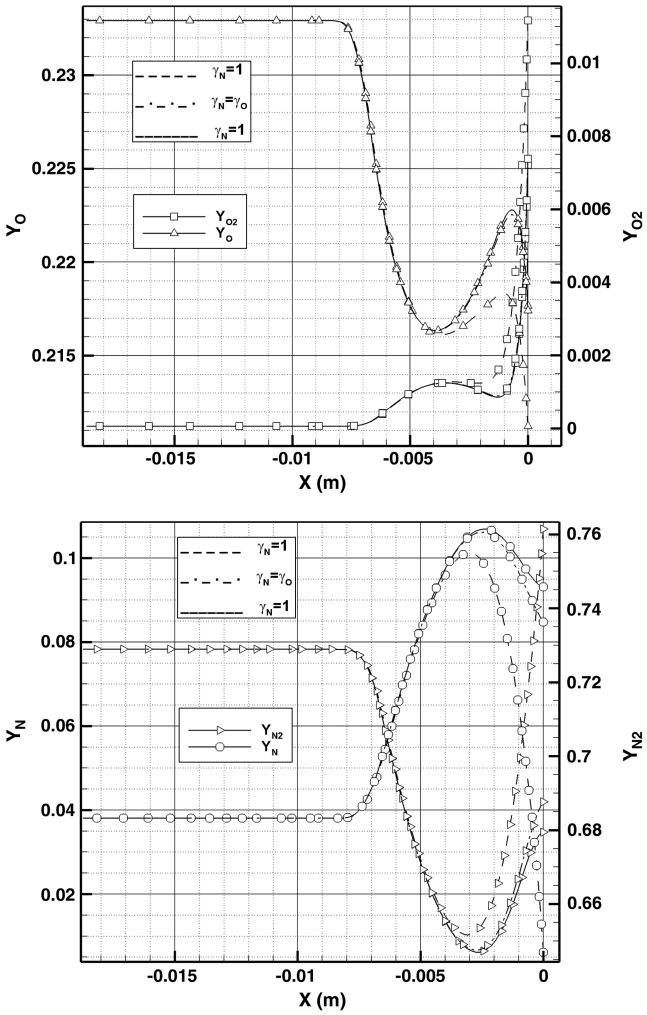

Fig. 12 Mass fraction profiles along the stagnation line; γ_O: PM1000 model; γ_N: PM1000 model, 0 and 1.

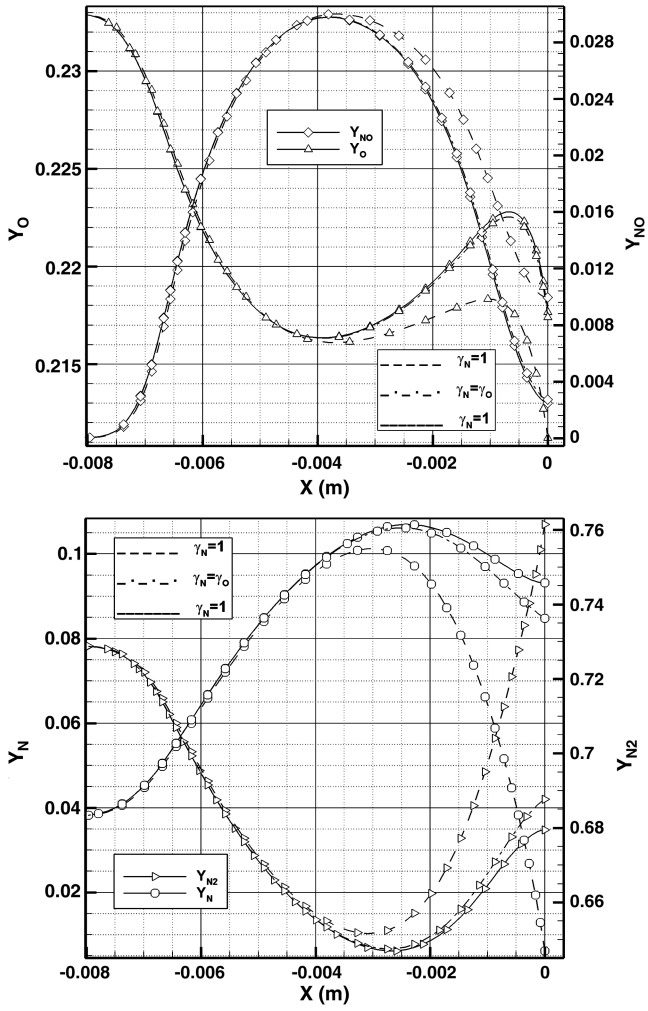

Fig. 13 Mass fraction profiles; stagnation region; γ_O: PM1000 model; γ_N: PM1000 model, 0 and 1.

The wall heat flux using the PM1000 model of Eq. (10) has been compared, in terms of total wall heat flux, with that by Stewart and Bouslog [17] in Figure 16, also including the two limit conditions of noncatalytic and fully catalytic walls. As expected from the measurements reported in [17], the model by Stewart and Bouslog predicts a more catalytic material, even though in that case measurements refer

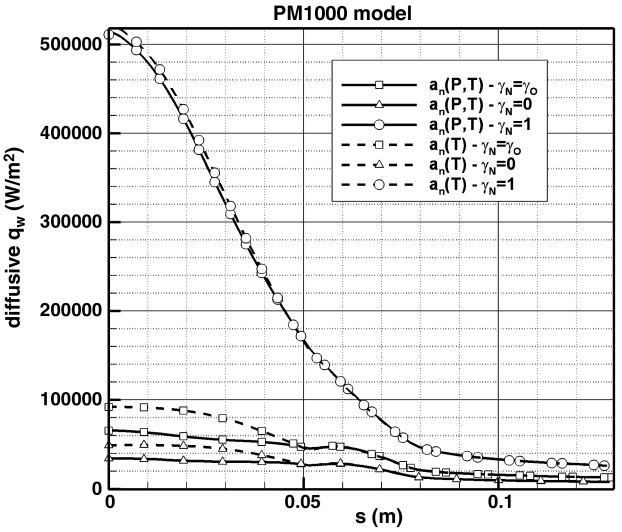

Fig. 15 Diffusive heat flux q_w on the sphere; comparison between PM1000 model formulations.

just to a single pressure (36 Pa) much lower than those tested by VKI and CNRS.

B. EXPERT Capsule Test Case

The second test case is an axisymmetric simulation of an EXPERT section at a point in its trajectory corresponding to maximum stagnation point heat flux ($h = 34.382$ km, $M = 13.512$, $Re/m = 2.7 \times 10^6$, $v = 5$ km/s, July 2008).

The C-SiC nose of the capsule has been assumed noncatalytic to be conservative with respect to the heat flux peak foreseen at the interface with PM1000, whereas for the C-SiC flap, the catalysis model by Stewart et al. has been adopted both for O and N [23]. For PM1000, this model has been implemented in the version $a_n(P, T)$, both for oxygen and for nitrogen recombination. In this case, the recombination of nitrogen does not play an important role in determining the wall heat flux, due to the small nitrogen concentration in correspondence of the PM1000 region.

The effect of the grid on the convergence of results (grid convergence) has been evaluated in terms of 1) heat flux at the catalytic interface between nose and plate (Q^*), 2) influence of the upstream flow, by means of D_u (i.e., the distance between the flap hinge line and the separation point on the plate), and 3) the downstream

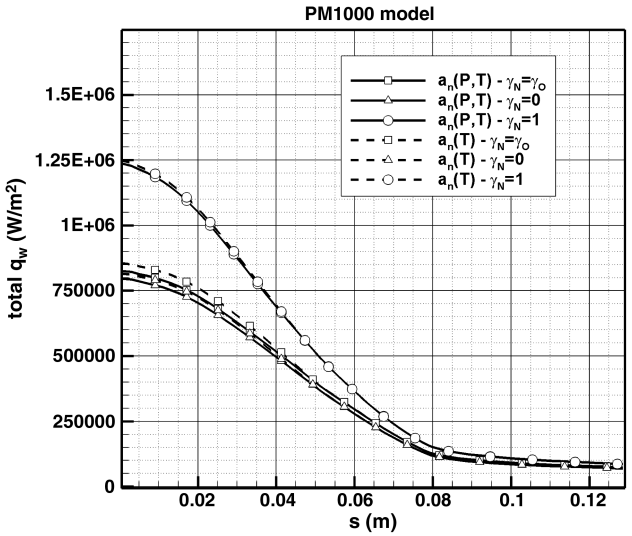

Fig. 14 Total heat flux q_w on the sphere; comparison between PM1000 model formulations.

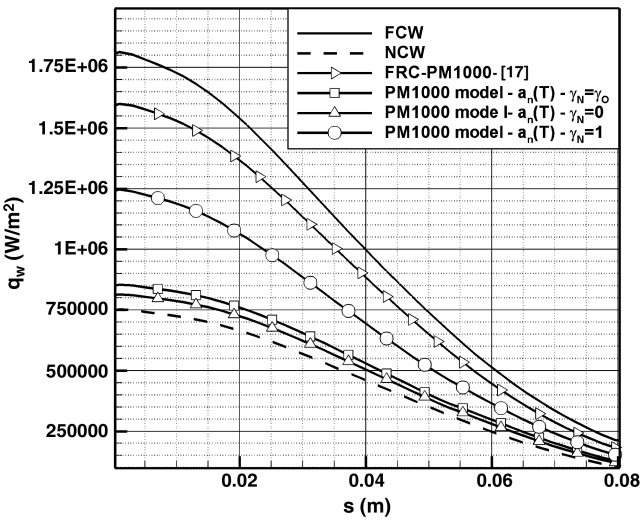

Fig. 16 Heat flux distribution on the sphere; comparison between wall catalysis conditions.

Table 3 Grids, number of cells, minimum spacing normal to the wall at the stagnation point, and aspect ratio

Grid	N	Δy_w, m	AR
1	1632	5.4E − 06	4918
2	6528	2.2E − 06	6039
3	26,112	1E − 06	6645
4	42,624	1E − 06	6645

Table 4 Parameters for the four grids and Richardson extrapolation values

Grid	$N^{-1/2}$	Q^*, W/m^2	D_u, m	D_d, m
1	0.0248	204,462.91	0.06	0.0635
2	0.0124	206,154.34	0.126	0.1121
3	0.0062	206,544.19	0.14	0.1167
4	0.0048	208,565.43	0.1411	0.1178
(Rich. extrap.)$_4$	0	209,048.43	0.1412	0.1182
GCI$_4$	——	0.069	0.0009	0.0039

influence via D_d (i.e., the distance between the flap hinge line and the reattachment point on the flap).

Convergence has been analyzed with the four grids of Table 3, where number of cells, minimum spacing normal to the wall at the stagnation point, and aspect ratio are also reported for each grid.

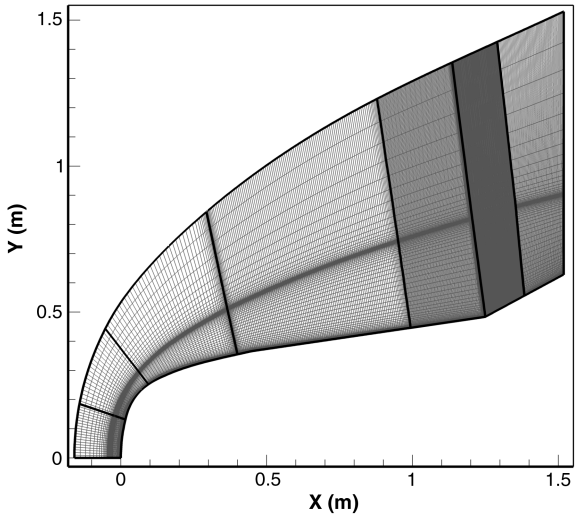

Fig. 17 Grid 3 of Table 3.

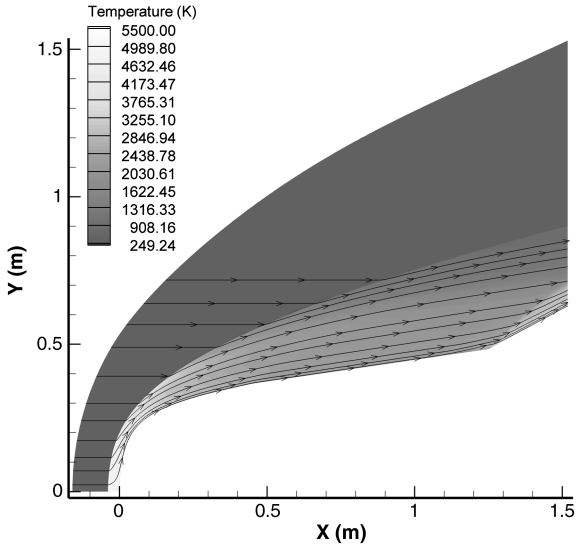

Fig. 18 Temperature contour map.

Each of the first three grids doubles the number of points in the two coordinate directions with respect to the previous grid (grid 3 is shown in Fig. 17); the fourth is refined near the most critical regions, namely the interface between the C-SiC nose and the plate, and the separation region due to the shock wave/boundary-layer interaction.

In Table 4, the computed values of Q^*, D_u, and D_d are reported for the four grids; the last line reports Richardson-extrapolated values. These are estimates of the "continuum value" (i.e., the value at zero grid spacing) obtained from a series of discrete values [24] defined as

$$f_{h=0} \cong f_{i+1} + \frac{f_{i+1} - f_i}{r^p - 1} \tag{11}$$

where $f_{h=0}$ is the value at zero grid spacing; f_i and f_{i+1} are the values computed on two grids, f_{i+1} being the finer; p is the order of convergence; and r is the grid refinement ratio:

$$p = \ell_n\left(\frac{f_{i+1} - f_i}{f_i - f_{i-1}}\right) / \ell_n(r) \tag{12}$$

$$r = \sqrt[3]{\frac{N_{i+1}}{N_i}} \tag{13}$$

where N_i. N_{i+1} are the numbers of cells of the two grids. In the following, N will be used to indicate the total number of cells of a grid, whereas $(1/N)^{1/2}$ represents adequately the grid resolution for a two-dimensional grid.

An error bar on the grid convergence of the solution computed on the ith grid is provided by the so-called grid convergence index (GCI):

$$\mathrm{GCI}_i = \frac{F_s \left| \frac{f_{i-1} - f_i}{f_i} \right|}{(r^p - 1)} \tag{14}$$

where F_s is a safety factor, which is assumed equal to 1.25.

The GCI computed for grid 4 is in Table 4; its value in correspondence of the parameters selected (Q^*, D_u, D_d) shows that results are clearly within the asymptotic range of convergence.

Results shown hereinafter refer to the finest grid level. The temperature contour map is shown in Fig. 18. Total wall heat flux, temperature, and pressure are plotted vs x in Fig. 19. Note the heat flux peak at the junction between nose and main capsule body, where a jump in catalytic conditions occurs. Slightly downstream, at the junction between the conical part and the flat plate, a sudden expansion occurs with a heat flux peak. An enlargement of the PM1000 plate is shown in Fig. 20, which reports the diffusive heat flux, temperature, pressure, and oxygen recombination coefficient

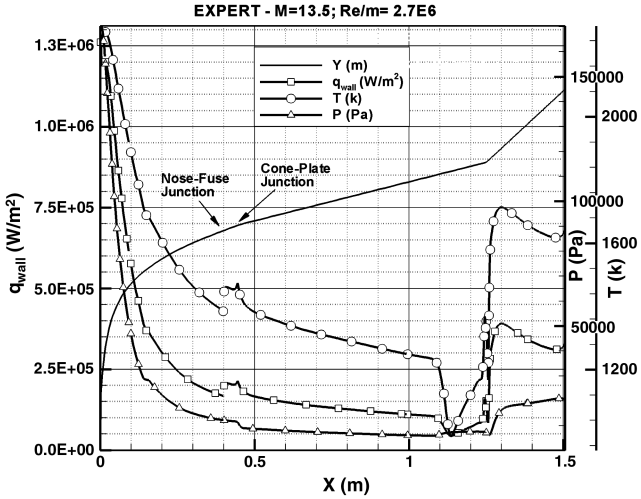

Fig. 19 Total wall heat flux, pressure, and temperature along x.

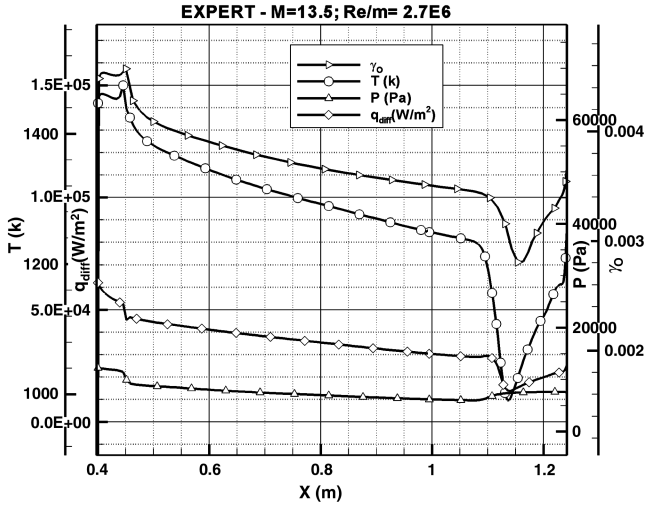

Fig. 20 Diffusive wall heat flux, pressure, temperature, and γ_O along PM1000 plate.

distributions. The diffusive heat flux distribution follows that of γ, which in turn mirrors that of the temperature and pressure profiles.

VI. Conclusions

A simplified catalysis model has been developed with the aim of defining a recombination coefficient even when detailed physical modeling approaches are unrealizable, namely when material characteristics are unknown. In this model, the recombination coefficient is calculated by trying to reproduce the main physics. In particular, a two-steps kinetics, which is characteristic of catalysis, has been formulated. The constants of the model have been calculated from experimental measurements at different pressures. This model has been successfully applied to PM1000 material, by using experimental measurements of oxygen recombination obtained in the VKI and CNRS facilities. Comparison with heat flux distributions obtained by assuming either complete noncatalytic or fully catalytic surface shows that, within the range of pressures of the experimental data, and within the assumption of the model, the PM1000 behaves as a low catalytic material. The available data are insufficient to fully characterize the material and the associated errors appear too large to allow designing a light or reasonably-sized TPS in a reliable manner: for this purpose, more data are definitely needed. However, the method devised and its application to realistic problems appears to work well with two test cases and is therefore promising.

Acknowledgments

The authors wish to acknowledge the partial financial support by the ESA multiphysics project monitored by F. Cipollini, to whom thanks are given for suggesting this work. Special thanks go to G. Rufolo of Centro Italiano Ricerche Aerospaziali for information on processing experimental data and for many useful discussions.

References

[1] Scott C. D., "The Effects of Thermochemistry Non-Equilibrium and Surface Catalysis in the Design of Hypersonic Vehicles," *Proceedings of the 1st Joint Europe-US Short Course on Hypersonics*, Vol. 2, edited by J. Bertin, and J. Periaux, Birkäuser, Boston, 1987, pp. 1–72.

[2] Billing, G. D., and Cacciatore, M., "Semiclassical Calculation of the Reaction Probability for the Processes $C + O \rightarrow CO$ on a Pt(111) Surface," *Chemical Physics Letters*, Vol. 113, No. 1, 4 Jan. 1985, pp. 23–28. doi:10.1016/0009-2614(85)85005-3

[3] Tully, J. C., "Dynamics of Gas-Surface Interactions: Reaction of Atom Oxygen with Adsorbed Carbon on Platinum," *Journal of Chemical Physics*, Vol. 73, No. 12, 15 Dec. 1980, pp. 6333–6342. doi:10.1063/1.440097

[4] Cacciatore, M., and Billing, G. D., "Dissociation and Atom Recombination of H_2 and D_2 on Metallic Surfaces: A Theoretical Survey," *Pure and Applied Chemistry*, Vol. 68, No. 5, 1996, pp. 1075–1081. doi:10.1351/pac199668051075

[5] Jackson, B., and Persson, M., "A Quantum Mechanical Study Recombinative Desorption of Atomic Hydrogen on a Metal Surface," *Journal of Chemical Physics*, Vol. 96, No. 3, 1 Feb. 1992, pp. 2378–2386. doi:10.1063/1.462034

[6] Cacciatore, M., Rutigliano, M., and Billing G. D, "Eley-Rideal and Langmuir-Hinshelwood Recombination Coefficients for Oxygen on Silica Surfaces," *Journal of Thermophysics and Heat Transfer*, Vol. 13, No. 2, April–June 1999, pp. 195–203. doi:10.2514/2.6436

[7] Nasuti, F., Barbato, M., and Bruno, C., "Material-Dependent Catalytic Recombination Modeling for Hypersonic Flows," *Journal of Thermophysics and Heat Transfer*, Vol. 10, No. 1, Jan.–March 1996, pp. 131–136. doi:10.2514/3.763

[8] Kurotaki, T., "Construction of Catalytic Model on SiO_2-Base Surface and Application on Real Trajectory," AIAA Paper 2000-2366, June 2000.

[9] Glassman, I., *Combustion*, 3rd ed., Academic Press, San Diego, CA, 1996, Chap. 2.

[10] Chazot, O., Collin, P., and Asma, C., "Steady State Testing of Pre-Oxidized PM1000 Material," von Karman Inst. 04/VKI/AR/OC/ARR0418/WP2, 2004.

[11] Chazot, O., Collin, P., and Asma, C., "TPS Plasma Tests for Analysis of the Gas-Surface Interaction: Steady-State Testing of Pre-Oxidized PM1000 Material-3rd Campaign," von Karman Inst. 05/VKI/AR/OC/ARR0305/WP2.1, 2005.

[12] Chazot, O., Collin, P., and Asma, C., "Synthesis and Recommendations for Future Improvements," von Karman Inst. 05/VKI/AR/OC/ARR0305/WP4, 2005.

[13] Chazot, O., Krassilchikoff, H. W., and Thömel, J., "TPS Ground Testing in Plasma Wind Tunnel for Catalytic Properties Determination," AIAA Paper 2008-1252, Jan. 2008.

[14] Chazot, O., "Experimental Studies on Hypersonic Stagnation Point Chemical Environment," *Proceedings of Experiment, Modeling and Simulation of Gas-Surface Interactions for Reactive Flows in Hypersonic Flights*, Vol. 1, edited by O. Chazot and P. Rini, von Karman Inst., Rhode-Saint-Genèse, Belgium, 2006, pp. 1–32.

[15] Balat-Pichelin, M., "Interaction of Reactive Gas Flows and Ceramics at High Temperature: Experimental Methods for the Measurement of Species Recombination During Planetary Entry," *Proceedings of Experiment, Modeling and Simulation of Gas-Surface Interactions for Reactive Flows in Hypersonic Flights*, Vol. 1, edited by O. Chazot and P. Rini, von Karman Inst., Rhode-Saint-Genèse, Belgium, 2006, pp. 12-1–2-25.

[16] Balat-Pichelin, M., and Badie, J., "Measurement of the Recombination Coefficient of Atomic Oxygen on the PM1000 Material," Centre National de la Recherche Scientifique 753423/00, 2005.

[17] Stewart, D., and Bouslog, S., "Surface Characterization of Candidate Metallic TPS for RLV," AIAA Paper 99-3458, June–July 1999.

[18] Curve Fitting Toolbox, User's Guide, MathWorks, 2007.

[19] Branch, M. A., Coleman, T. F., and Li, Y., "A Subspace, Interior, and Conjugate Gradient Method for Large-Scale Bound-Constrained Minimization Problems," *SIAM Journal on Scientific Computing*, Vol. 21, No. 1, 1999, pp. 1–23. doi:10.1137/S1064827595289108

[20] Ranuzzi, G., and Borreca, S., "CLAE Project. H3NS: Code Development and Validation," Centro Italiano Ricerche Aerospaziali, CIRA-CF-06-1017, Sept. 2006.

[21] Di Clemente, M., "Numerical Studies for the Realization of Aerodynamic Systems for Guide and Control of Re-Entry Vehicles," Ph.D. Dissertation, Mechanics and Aeronautics Dept., Univ. of Rome, "La Sapienza," Rome, 2008.

[22] Rufolo, G. C., "Standard Model Testing: Flow Characterization in Scirocco," Centro Italiano Ricerche Aerospaziali, CIRA-TR-03-561, Nov. 2003.

[23] Stewart, D., Henline, W., and Chen, Y., "Effect of Non-Equilibrium Flow Chemistry and Surface Catalysis on Surface Heating to AFE," AIAA Paper 91-1373, June 1991.

[24] Roache, P. J., *Verification and Validation in Computational Science and Engineering*, Hermosa, Albuquerque, NM, 1998.

[25] Park, C., "A Review of Reaction Rates in High Temperature Air," AIAA Paper 89-1740, June 1989.

[26] Millikan, R. C., and White, D. R., "Systematic of Vibrational

Relaxation," *Journal of Chemical Physics*, Vol. 39, No. 12, 1963, pp. 3209–3213.
doi:10.1063/1.1734182

[27] Park, C., "Validation of Multi-Temperature Nozzle Flow Code NOZNT," AIAA Paper 93-2862, 1993.

[28] Yun, K. S., and Mason, E. A., "Collision Integrals for the Transport Properties of Dissociating Air at High Temperatures," *Physics of Fluids*, Vol. 5, No. 4, 1962, pp. 380–386.
doi:10.1063/1.1706629

[29] Kee, R. J., Warnatz, J., and Miller, J. A., "A Fortran Computer Code Package for the Evaluation of Gas-Phase Viscosities, Conductivities and Diffusion Coefficients," Sandia Rept. SAND83-8209, March 1983.